Anomalous ANITA air shower events and tau decays

Shoshana Chipman and Rebecca Diesing

Department of Astronomy and Astrophysics, University of Chicago, Chicago, Illinois 60637, USA

Mary Hall Reno

Department of Physics and Astronomy, University of Iowa, Iowa City, Iowa 52242, USA

Ina Sarcevic

Department of Physics, University of Arizona, 1118 E. 4th St. Tucson, Arizona 85704, USA

Two unusual neutrino events in the Antarctic Impulse Transient Antenna (ANITA) appear to have been generated by air showers from a particle emerging from the Earth at angle $\sim 25°$–$35°$ above the horizon. We evaluate the effective aperture for ANITA with a simplified detection model to illustrate the features of the angular dependence of expected events for incident standard model tau neutrinos and for sterile neutrinos that mix with tau neutrinos. We apply our sterile neutrino aperture results to a dark matter scenario with long-lived supermassive dark matter that decay to sterile neutrinolike particles. We find that for upgoing air showers from tau decays, from isotropic fluxes of standard model, sterile neutrinos, or other particles that couple to the tau through suppressed weak interaction cross sections cannot be responsible for the unusual events.

I. INTRODUCTION

Neutrinos of astrophysical origin present the opportunity to explore and understand the conditions of cosmic ray acceleration and the surrounding astrophysical environment [1,2]. A number of detectors, current and proposed, rely on neutrino interactions in water or ice. Detectors include IceCube [3], ANTARES [4], KM3net [5], ARA [6], and ARIANNA [7]. Air shower signals via particles, fluorescence, radio, and optical Cherenkov are the target of surface instruments such as Auger [8–10], the Telescope Array [11], MAGIC [3], GRAND [12], and Trinity [13]. Above the Earth, proposed satellite-based instruments sensitive to upward-going air showers include CHANT [14] and POEMMA [15]. The balloon-borne Antarctic Impulse Transient Antenna (ANITA) detector [16–19] is sensitive to neutrino interactions in the Antarctic ice where the Askaryan effect is important. ANITA is also sensitive to tau neutrino charged current interactions in the Earth that produce taus that decay in the atmosphere. These upward-going tau shower signals at ANITA are the focus of this paper.

For neutrino telescopes, the standard model source of taus is tau neutrino charged-current interactions in the Earth. With neutrinos coming from charged pion decays and nearly bimaximal $\nu_\mu - \nu_\tau$ mixing, over astronomical distances approximately equal fluxes of electron neutrinos, muon neutrinos, and tau neutrinos arrive at the Earth [20]. Lepton flavor universality has the three standard model neutrinos with equal interaction cross sections on nucleon targets and, at high energies, the neutrino and antineutrino

cross sections are equal [21–25]. Below, "neutrino" refers to both particle and antiparticle.

The ANITA Collaboration has reported observations of two unusual events that are consistent with shower characteristics of upward-going taus that decay in the atmosphere [18,19]. In the ANTIA-III run, event 15717147 had an estimated shower energy of $0.56^{0.3}_{-0.2} \times 10^9$ GeV and arrived at the detector with an angle of $-35.0° \pm 0.3°$ (below the horizontal)—which is to say that the event emerged from the Earth at $\sim 34.5°$ above the horizon, or $\sim 55.5°$ from the vertical [19]. Additionally, the first run of ANITA in 2016 produced event 3985267, of shower energy of $(0.6 \pm 0.4) \times 10^9$ GeV, which arrived at the detector with an angle of $-27.4° \pm 0.3°$, a $\sim 26.8°$ emergence angle [18]. The interpretation of these unusual events as coming from tau neutrinos is problematic [18,19,26] because of the energies of the showers and the apparent angles of the tau neutrinos that induced them.

One challenge to the tau neutrino interpretation is neutrino flux attenuation. While governed by weak interactions, the neutrino interaction length (in units of column depth) $\lambda_\nu = (N_A \sigma_{\nu N})^{-1}$ [21–25] is large compared to the column depths traversed by the neutrino trajectories of the unusual events. As an indication of the scales involved, for example, for a neutrino incident at nadir angle $0°$, the column depth is $\sim 1.1 \times 10^{10}$ g/cm^2, equal to the neutrino interaction length for $E_\nu \sim 40$ TeV. For a nadir angle of $60°$ (elevation angle $40°$), the neutrino interaction length equals the column depth in Earth when $E_\nu \sim 250$ TeV.

As the neutrino energy increases, the effective solid angle that can be detected decreases. The neutrino fluxes incident at small nadir angles, or alternatively, emerging at large elevation angles, can be significantly attenuated. At the elevation angles of 25°–35° of the high energy ANITA events, the tau exit probability is small in the standard model. Additionally, it is difficult to explain why events are detected at large elevation angles but not small elevation angles where the exit probabilities are larger [26–28].

Physical effects related to the ice/air boundary for downward-going cosmic ray air showers are under discussion as possible explanations of ANITA's unusual events [29,30]. For example, explanations point toward the Antarctic subsurfaces and firn density inversions as well as the ice structure as a possible explanation [30]. A beyond the standard model (BSM) explanation proposed for downward-going air showers is axion-photon conversion [31].

There are also a number of BSM physics explanations for upward-going air showers that come from tau decays or other particle decays in the atmosphere. Neutrino production of heavy BSM particles that decay directly to taus or to other BSM particles that couple to taus have been introduced to modify the standard model large elevation angle suppression [27,32–35]. Several scenarios with decaying heavy dark matter have been proposed, including the one in which decaying dark matter is trapped in the Earth [36], and others in which the dark matter decays in the galactic halo that ultimately produce shower [28,37,38] or Askaryan events [39] in ANITA. Sterile neutrinos that interact to produce taus have been proposed to avoid the neutrino flux attenuation at large elevation angles [40,41].

In general, the ANITA events are in tension with other constraints, for example, as discussed in Ref. [38]. While there are scenarios that may be acceptable, e.g., boosted dark matter decays into lighter dark matter which decays into hadrons for specific model parameters [37], it is a challenge to describe the ANITA unusual events including the emergence angles and not over predict IceCube and Auger event rates.

Most of the BSM analyses use approximate analytic results and a narrow energy range associated with ANITA's unusual events. In this paper, we consider a range of energies and angles using Monte Carlo simulations of neutral particle interactions that couple to taus and a stochastic evaluation of tau energy loss in the Earth [42]. Using a simplified model of the ANITA detection probability, we find the angular dependence of the effective aperture. Our analysis allows us to separate the particle physics effects (both standard model and a sterile neutrino example of BSM physics) from the tau air shower, detection, and surface geometry effects in the evaluation of the effective aperture.

We start with the standard model evaluation of the tau exit probabilities. We also consider a modification of the standard model tau neutrino cross section with a suppression

associated with a color glass condensate treatment of the high energy extrapolation of the neutrino-nucleon cross section [43–48]. The "sterile neutrino" considered here is a generic neutral BSM particle with suppressed cross sections, assumed to couple to taus by charged current interactions with a cross section $\sigma_{\nu_s N} = \epsilon_\nu \sigma_{\nu N}$.

We conclude that standard model ν_τ's from an isotropic flux cannot account for the unusual events. Our results are consistent with those of Ref. [26] and others [28,30,38]. Our quantitative evaluation of the exit probabilities for τ's from sterile neutrino interactions in the Earth demonstrates that even with no flux attenuation in the Earth, the lack of events at lower elevation angles makes even a large isotropic flux of sterile neutrinos a poor candidate source of the ANITA unusual events. We find that in principle an energy threshold effect can enhance large elevation angle events relative to small angles. A monoenergetic source in the energy threshold region that may produce upward-going air showers, the feebly interacting χ from supermassive dark matter in the model of Hooper et al. in Ref. [39], is used as an example to demonstrate this effect.

In the next section, we outline our approximate evaluation of the effective aperture for standard model neutrinos and for sterile neutrinos with suppressed cross sections. We discuss the geometric and neutrino interaction origins of the angular distribution of the effective aperture. In Sec. III, we discuss how signals at large elevation angles may be enhanced by showers with energies near the ANITA energy threshold. We demonstrate the effect with a sterile neutrino example and ~400 PeV supermassive dark matter decays in the galactic halo [39]. A related IceCube signal is a constraining feature. Finally, we summarize our results in Sec. IV.

II. EFFECTIVE APERTURE

A. Overview

The first step in determining an event rate is finding the effective aperture for ANITA. The ANITA effective aperture $\langle A\Omega \rangle$ depends on the viewable area of the Earth below the detector and on the probability to observe a tau decay induced air shower at a given angle and altitude. The geometry is illustrated in Figs. 1 and 2. The ANITA detector is at altitude h, taken to be $h = 35$ km [26]. The signals considered here come from air showers along the trajectory of an emerging tau that makes an angle $\theta_{\rm tr}$ with respect to the local normal $\hat{n}$ at its point of emergence from the Earth, which is at a colatitude θ_E relative to the line from the center of the Earth to ANITA. The viewing angle θ_v is the angle from ANITA to the point at which the tau emerges. It is convenient to describe elements of the observation probability in terms of the tau elevation angle $\beta_{\rm tr}$, related to the trajectory's angle to $\hat{n}$ by

$$\beta_{\rm tr} + \theta_{\rm tr} = \pi/2. \tag{1}$$

The effective aperture for incident tau neutrinos of energy E_{ν_τ} can be written as [49]
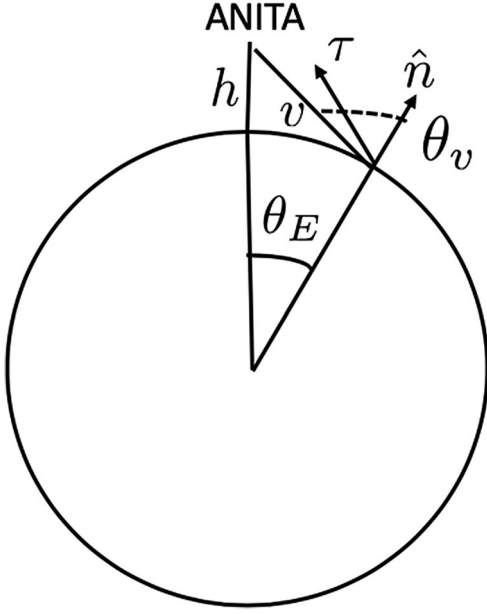
FIG. 1. Geometry of ANITA an altitude h above the surface of the Earth. The line of sight from the tau exit point at a colatitude θ_E has length v and makes an angle θ_v relative to the local normal $\hat{n}$.

$$\langle A\Omega(E_{\nu_\tau})\rangle = \int_S \int_{\Delta\Omega_{\rm tr}} P_{\rm obs}\hat{r}\cdot\hat{n}dSd\Omega_{\rm tr}, \qquad (2)$$

where $\hat{r}\cdot\hat{n} = \cos\theta_{\rm tr}$, $P_{\rm obs}$ is the detection probability, and dS is the area element on the surface of the Earth. The integral $d\Omega_{\rm tr}$ accounts for the trajectories of the tau for which the air shower is detected.

The effective Cherenkov angle is $\theta_{\rm Ch}^{\rm eff} \sim 1°$. In all that follows, we approximate $\theta_{\rm tr} \simeq \theta_v$ since Cherenkov angle is small. This simplifies the evaluation of the effective aperture. The effective aperture is then approximately [49] (see also, Ref. [42], Appendix A)
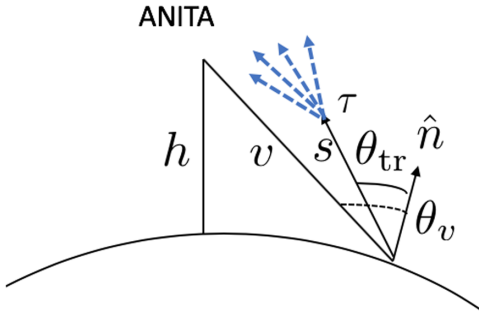

FIG. 2. The tau trajectory makes an angle $\theta_{\rm tr}$ relative to the local normal $\hat{n}$. The tau decays a distance s along its trajectory. The figure is exaggerated to distinguish θ_v and $\theta_{\rm tr}$; however, the effective Cherenkov angle of the signal from the tau decay shower is such that $\theta_v \simeq \theta_{\rm tr}$.

$$\langle A\Omega(E_{\nu_\tau})\rangle \simeq 2\pi^2 R_E^2 \sin^2\theta_{\rm Ch}^{\rm eff} \int P_{\rm obs}\cos\theta_v \sin\theta_E d\theta_E. \qquad (3)$$

The radius of the Earth is $R_E = 6371$ km.

The probability $P_{\rm obs}$ that a tau neutrino with energy E_{ν_τ} produces a shower that is detectable is [26,50]

$$P_{\rm obs} = \int p_{\rm exit}(E_\tau|E_{\nu_\tau}, \theta_{\rm tr})$$

$$\times \left[\int ds\, p_{\rm decay}(s)P_{\rm det}(E_\tau, \theta_v, \theta_{\rm tr}, s)\right]dE_\tau. \qquad (4)$$

As noted above, we approximate $\theta_v \simeq \theta_{\rm tr}$ in the discussion below. For $p_{\rm decay}$ and $P_{\rm det}$, the distance s is the length of the tau path length from its exit point on Earth to its point of decay.

In the next section, we discuss the exit probabilities and emerging tau energies as a function of $\beta_{\rm tr}$ for the standard model and variations. The decay and detection probabilities for tau decays are independent of exit probabilities. The decay probability density is

$$p_{\rm decay} = \frac{\exp(-s/(\gamma c\tau))}{\gamma c\tau}, \qquad (5)$$

where $\gamma = E_\tau/m_\tau c^2$ is the usual gamma-factor of time dilation for tau decays. The decay length of the tau is $\gamma c\tau \simeq 5$ km $\times (E_\tau/10^8$ GeV$)$.

For the detection probability, we use a simplified model of the ANITA-III detector. ANITA detects the electric field generated by the shower. We approximately follow Ref. [32]. We take the probability of detection of an upgoing air shower from a tau decay, with energy $E_{\rm shr}$, as the product of Heaviside step functions times the hadronic branching fraction of the tau $B_{\rm had} = 0.648$,

$$P_{\rm det}(E_\tau, \beta_{\rm tr}) = B_{\rm had}\Theta\left(\frac{E_{\rm shr}}{10^8\text{ GeV}}\frac{74\text{ km}}{r_0(E_\tau, s_d, \beta_{\rm tr})} - 1\right)$$

$$\times \Theta(6\text{ km} - a). \qquad (6)$$

The first Heaviside step function enforces a minimum electric field requirement which to first approximation follows from the fact that higher shower energies have larger electric fields. Up to a point, the shorter the distance from the start of the shower to ANITA, $r_0 \simeq v - s$, the larger the electric field at the antennas. The second Heaviside step function cuts off the integration over altitude at 6 km. As the altitude at which a tau shower begins is increased, first the electric field gets larger, but after ~6 km, the angle between the shower axis and line of sight ($\theta_{\rm view}$ in Ref. [26]) decreases [26].

Equation (6) is a rough approximation to a more detailed model of the electric field from tau showers [26]. We show below that using Eq. (6) with $E_{\rm shr} = 0.98E_\tau$ as in Ref. [26] and

$$\theta_{\text{Ch}}^{\text{eff}} \simeq 1.0° - 0.02\beta_{\text{tr}}, \qquad (7)$$

for β_{tr} in degrees, the mean ANITA-I,III effective aperture is reasonably well reproduced.

B. Exit probability and effective aperture

The quantity $p_{\text{exit}}(E_\tau|E_{\nu_\tau}, \theta_{\text{tr}})$ is the exit probability density, which depends on the neutrino-nucleon cross section. The exit probability is

$$P_{\text{exit}}(E_{\nu_\tau}, \theta_{\text{tr}}) = \int dE_\tau(E_\tau|E_{\nu_\tau}, \theta_{\text{tr}}). \qquad (8)$$

Our standard model cross section for neutrino-isoscalar nucleon scattering is calculated with the CT14 parton distribution functions [51]. The cross section is shown with the solid blue line in Fig. 3. We use cumulative distribution functions to sample the energy distribution of the taus that exit for a given incident tau neutrino energy E_{ν_τ} and angle β_{tr}, as described in detail in Ref. [42].

The exit probability also depends on the tau electromagnetic energy loss. In charged current scattering, a tau is produced. The tau loses energy primarily through electron-positron pair production and photonuclear interactions, which we implement with a Monte Carlo simulation [52] that also includes tau neutrino regeneration. We use the Abramowicz *et al.* (ALLM) parameterization of the electromagnetic structure function F_2 [53,54] in our evaluation of the photonuclear contribution. At high energies, extrapolations of F_2 beyond the measured regime introduce uncertainties.

A feature unique to tau neutrinos is the significance of tau neutrino regeneration with neutrino interactions in the

Earth [42,55–60]. Tau neutrino regeneration comes from tau neutrino charged-current production of taus which subsequently decay back to ν_τ. Through a series of neutrino interaction and decay, high energy tau neutrinos can produce taus that emerge from the Earth to produce upgoing air showers [61–75]. More details on the evaluation of the tau exit probabilities appear in Ref. [42].

The upper panel of Fig. 4 shows the tau exit probabilities for fixed energies as functions of the elevation angle of the exiting tau, β_{tr}. The resulting effective aperture comes from the exit probabilities and the associated cumulative distribution functions for the exiting tau energies, together with the decay and detection probabilities. A comparison of our calculated effective aperture (solid line) and the mean ANITA I,III effective aperture from Ref. [26] (dashed line) in the lower panel of Fig. 4 shows that our simplified model of the ANITA detection probability is reasonable.

FIG. 4. *Upper*: the probability of a tau to exit for fixed $E_{\nu_\tau} = 10^8$, 10^9, 10^{10}, and 10^{11} GeV in the standard model, as a function of elevation angle β_{tr}. The ALLM photonuclear energy loss is used. *Lower*: the standard model effective aperture compared with the mean effective aperture of Anita I,III [26] for upward-going tau air showers from incident ν_τ's.
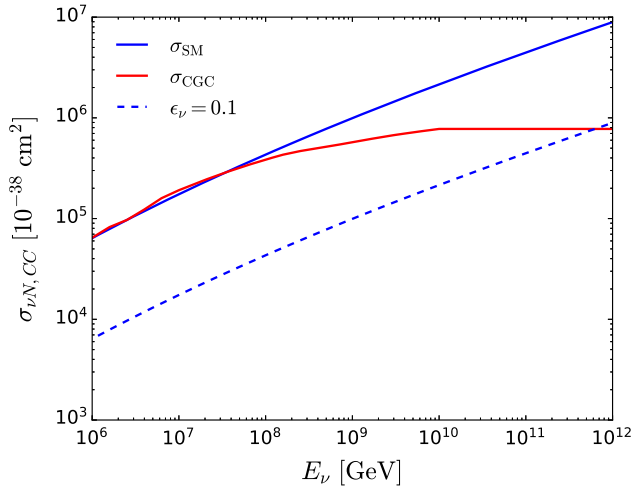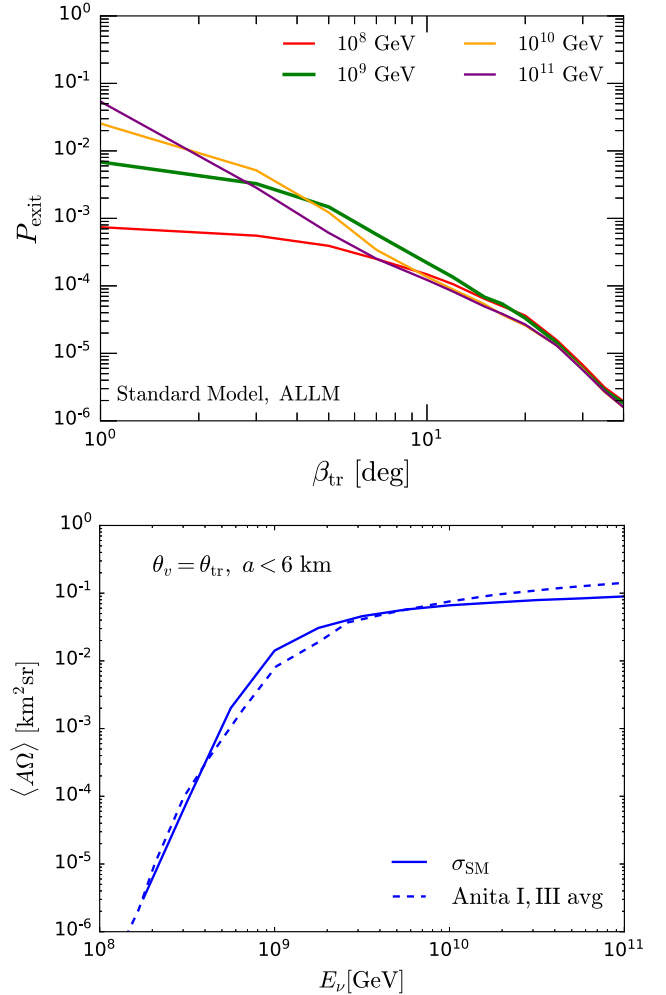

FIG. 3. The neutrino-nucleon charged current cross section as a function of neutrino energy for an evaluation using CT14 [51] parton distribution functions (SM), with color glass condensate suppression at high energies (CGC) [48] and for $\sigma = \epsilon_\nu \sigma_{\text{SM}}$ with $\epsilon_\nu = 0.1$.

Smaller cross sections, either from saturation effects for standard model neutrinos or for sterile neutrinos with a suppressed cross section, change the angular dependence of $p_{\text{exit}}(E_\tau | E_{\nu_\tau} \beta_{\text{tr}})$ because neutrino attenuation is reduced. We assume that the differential cross section, relatively normalized with a suppression factor of ϵ_ν, is the same as for the standard model evaluated with CT14 parton distribution functions. The charged current cross section with $\epsilon_\nu = 0.1$ is shown in Fig. 3. Smaller cross sections also result in fewer tau regeneration effects as the neutrino propagates through long chord lengths in the Earth. The first interaction occurs deeper along the neutrino trajectory.

High energy extrapolations of the neutrino-nucleon cross section eventually face unitarity limits on the growth of the cross section. In the parton picture, the high density of gluons at small parton momentum fraction x is such that gluon recombination occurs, eventually saturating the cross section. One approach to handle the saturation effects is the color glass condensate (CGC) formalism [43–48]. The high energy CGC extrapolation of the neutrino cross section is shown in Fig. 3 by the dashed red curve. This represents the strongest saturation effects presented in Ref. [48]. Figure 5 shows that the CGC extrapolation of the neutrino cross section has some impact on the exit probability at large angles and at high energies. Overall, the exit probabilities still fall with increasing β_{tr} in the range of tens of degrees.

We now turn to the sterile neutrino cross section. Figure 6 shows the tau exit probabilities (upper) and average energy of the emerging taus (lower) for a sterile neutrino cross section $\sigma_{\nu_s N} = \epsilon_\nu \sigma_{\nu N}$, with $\epsilon_\nu = 0.1$ (solid lines) and for the standard model (dashed lines). We assume that the sterile neutrino interactions convert sterile neutrinos to tau neutrinos.
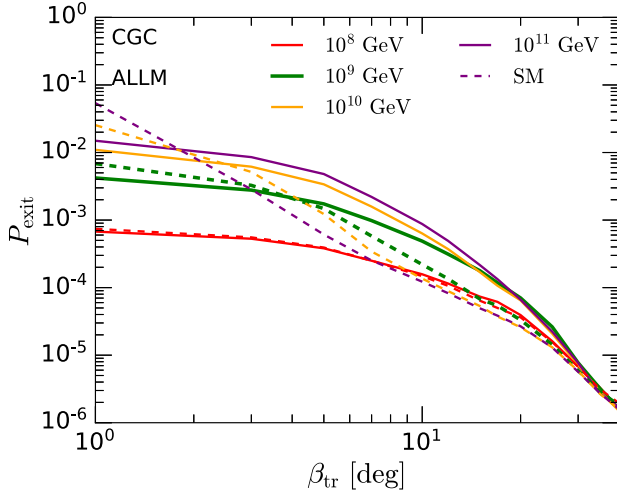
For small elevation angles (e.g., $\beta_{\text{tr}} = 1°$), attenuation is not important. The smaller cross section for the sterile neutrino reduces the standard model tau exit probability by ϵ_ν. At larger angles, the exit probabilities for the sterile neutrino scenario do not fall as quickly as for the standard model because the sterile interaction length is longer. For $E_{\nu_s} = 10^9$ GeV, the exit probability for $\epsilon_\nu = 0.1$ is more than an order of magnitude larger than for the standard model for $\beta_{\text{tr}} = 30°$.

The lower panel in Fig. 6 shows $\langle E_\tau \rangle$ as a function of β_{tr} for fixed E_{ν_τ}. The figure illustrates a second feature for $\epsilon_\nu = 0.1$ that enhances tau shower detectability at large elevation angles. At $\beta_{\text{tr}} = 30°$, for $E_{\nu_s} = 10^9$ GeV and $\epsilon_\nu = 0.1$, the average energy of the emerging tau is $\sim 3 \times 10^8$ GeV, an energy more likely to be detected than the average energy of $\sim 2 \times 10^7$ GeV of the standard model

FIG. 5.   The probability for a tau to exit for fixed $E_{\nu_\tau} = 10^8$, 10^9, 10^{10}, and 10^{11} GeV for the color glass condensate ultrahigh energy neutrino cross section extrapolation (solid lines) and for a parton distribution function evaluation of the cross section (σ_{SM}, dashed lines), as in Fig. 4.
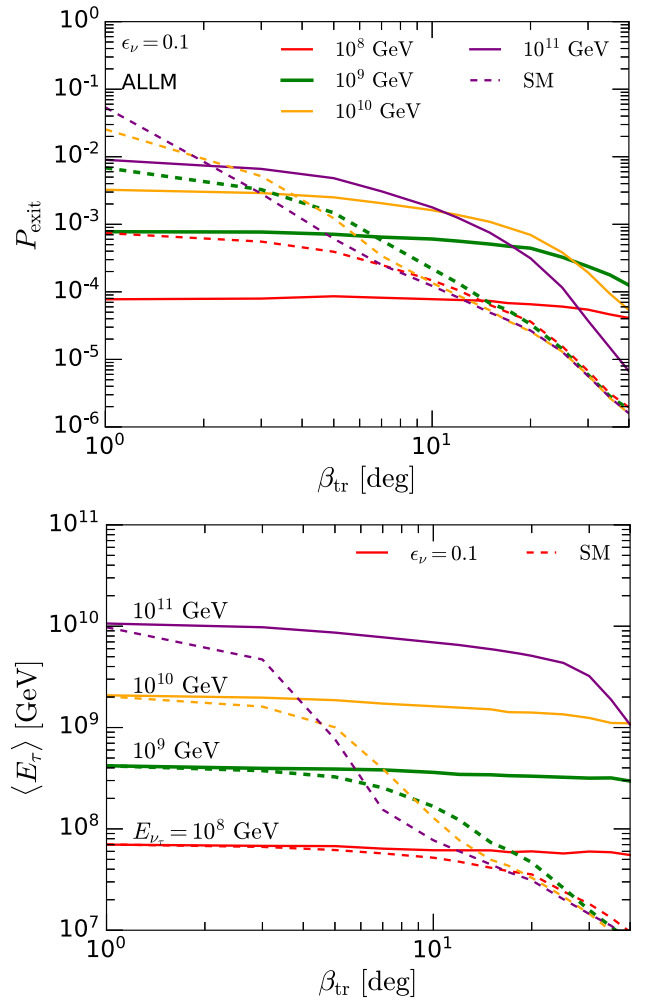
FIG. 6.   *Upper*: probabilities for fixed sterile neutrinos energies as a function of elevation angle, for an $\epsilon_\nu = 0.1$ sterile factor (solid lines) and for the standard model (dashed lines), using the ALLM model for photonuclear energy loss of the tau. *Lower*: the average energy of the emerging tau for sterile neutrinos with $\epsilon_\nu = 0.1$ and the standard model.
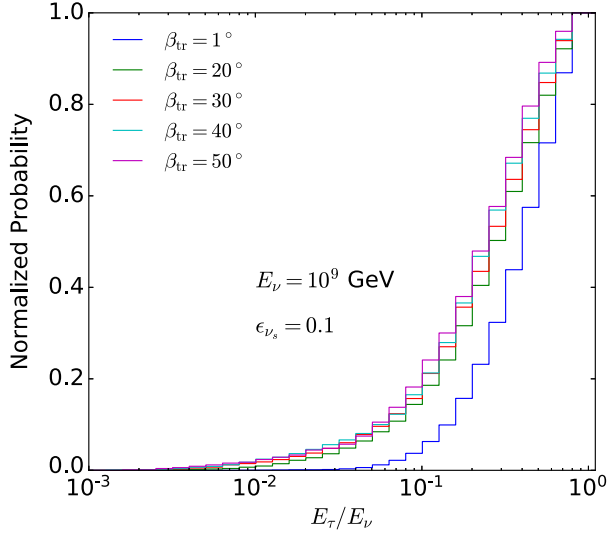
FIG. 7.   The cumulative distribution functions for several values of β_{tr} given $E_{\nu_s} = 10^9$ GeV and $\epsilon_\nu = 0.1$.

for the same incident neutrino energy and angle. The nearly constant $\langle E_\tau \rangle$ is evident from the cumulative distribution functions for exiting taus given a series of angles β_{tr} for a sterile neutrino energy $E_\nu = 10^9$ GeV, shown in Fig. 7.

Figure 8 shows the effective aperture for standard model tau neutrinos with the CT14 cross section (solid line, labeled σ_{SM}) and color glass condensate cross section (dot-dashed line, labeled CGC), and for sterile neutrinos with $\epsilon = 0.1, 0.01$ (dashed lines). The CGC effective aperture is slightly larger than the standard model evaluation at low energies and slightly lower than the standard model evaluation at high energies. The effective apertures
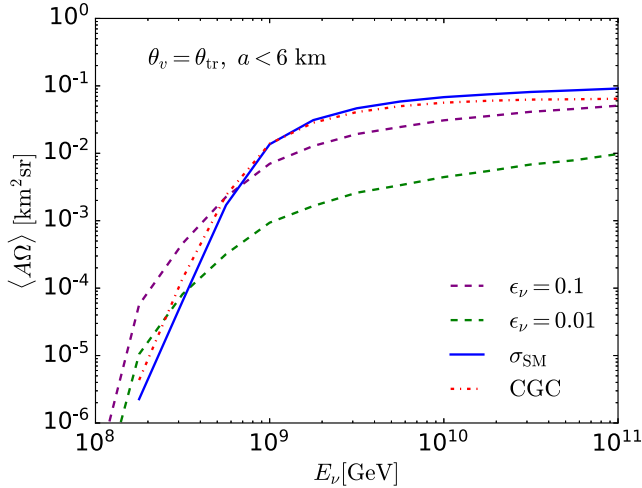

FIG. 8.   The effective aperture for standard model tau neutrinos and sterile neutrinos with $\sigma = \epsilon_\nu \sigma_{SM}$, with $\epsilon_\nu = 0.1$ and the ALLM energy loss model. Also shown is the acceptance with a modified neutrino cross sections according to the color glass condensate model (CGC).
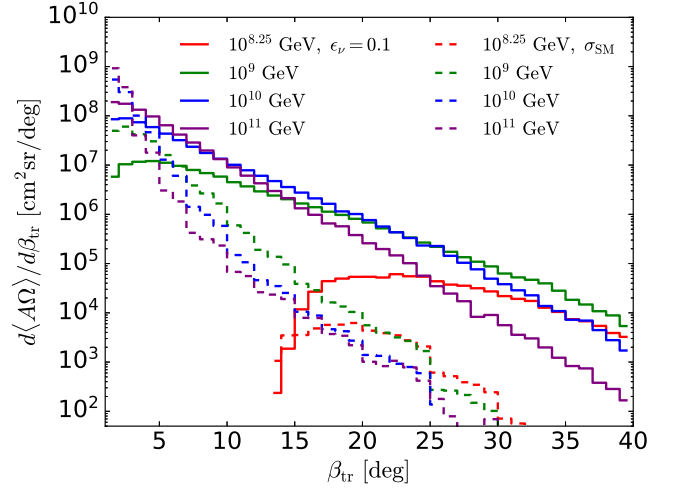

FIG. 9.   The differential effective aperture as a function of β_{tr} for standard model tau neutrinos (dashed) and sterile neutrinos (solid) with $\sigma = \epsilon_\nu \sigma_{SM}$, $\epsilon_\nu = 0.1$, and the ALLM energy loss model.

for $\epsilon = 0.1, 0.01$ are enhanced at low energies where the effective aperture increases with energy, but the maximum effective aperture is lower than for σ_{SM}.

The differential $\langle A\Omega \rangle$ as a function of β_{tr} is a useful diagnostic of the angular distribution of upward-going tau decay events [26]. There is not a significant change to angular distributions of predicted events using the CGC extrapolation of the neutrino cross section compared to the standard evaluation, so we do not show it here. For sterile neutrinos, the angular distribution changes, as shown in Figs. 9 and 10, for $\epsilon_\nu = 0.1$ and $\epsilon = 0.01$, respectively.

The enhanced high β_{tr} distribution, $d\langle A\Omega \rangle / d\beta_{tr}$, for $\epsilon_\nu = 0.1$ is shown with the solid lines in Fig. 9. The standard
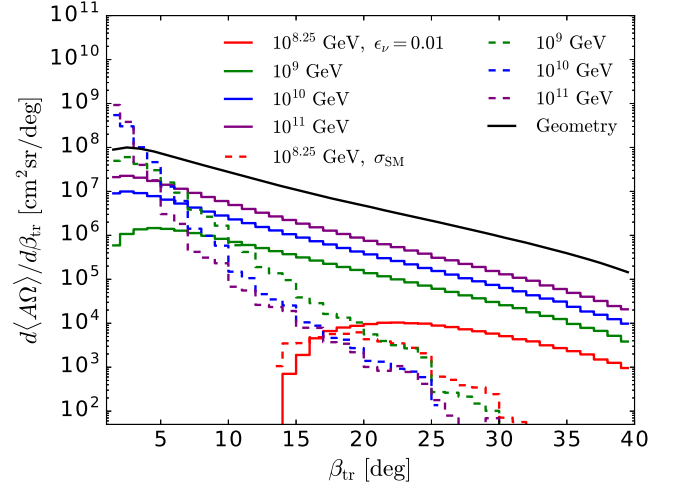

FIG. 10.   The differential effective aperture as a function of β_{tr} for standard model tau neutrinos (dashed) and sterile neutrinos (solid) with $\sigma = \epsilon_\nu \sigma_{SM}$, $\epsilon_\nu = 0.01$, and the ALLM energy loss model. The curve labeled "geometry" shows the rescaled differential aperture when $P_{exit} = P_{obs} = 1$.

model result is shown with the dashed lines. For $\beta_{\rm tr} = 30°$, the differential effective aperture as a function of $\beta_{\rm tr}$ is $\sim 10^2$–10^3 times larger for sterile neutrinos with $\epsilon = 0.1$ than for tau neutrinos. Figure 9 also shows that for $E_\nu = 10^9$ GeV and $\beta_{\rm tr} = 5°$, the differential effective aperture is the same for standard model and sterile neutrinos with $\epsilon_\nu = 0.1$, both larger by a factor of ~ 100 compared to the differential aperture for sterile neutrinos with $\epsilon_\nu = 0.1$ at $\beta_{\rm tr} = 30°$.

The larger differential aperture for small $\beta_{\rm tr}$ compared to $\beta_{\rm tr} \sim 30°$ is qualitatively a consistent feature for all sterile neutrino cross sections, as we illustrate with $\epsilon = 0.01$ in Fig. 10 with the solid histograms. For reference, we also show the standard model differential aperture, again with dashed histograms.

When $\epsilon_\nu = 0.01$, except for $E_{\nu_s} \sim 10^{11}$ GeV, there is little angular dependence in $P_{\rm exit}$. For ANITA, with our model of the effective aperture, essentially all of the angular dependence is in the angle integrals over θ_E and in $\theta_{\rm Ch}^{\rm eff}$, once the shower threshold energy is reached.

This effect can be understood by comparing the histograms in Fig. 10 with the black line labeled "geometry." The solid black line comes from a rescaled geometric differential aperture, where $P_{\rm obs} = 1$ and $P_{\rm exit} = 1$ for all angles. For high sterile neutrino energies, $P_{\rm obs} \simeq 1$. For low energies, at low angles, the showers cannot be detected because of the long distance from tau exit point to ANITA. The distance from the exit point to ANITA for $\beta_{\rm tr} = 1°$ is $v = 567$ km, while the decay length of the tau is $\gamma c\tau = 5$ km for $E_\tau = 10^8$ GeV. At high energies, the solid histograms in Fig. 10 increase with energy (for $\beta_{\rm tr} \gtrsim 5°$) with a scaling that follows the energy dependence of the neutrino cross section, but the shape follows the geometric differential aperture.

To further illustrate the geometric effect, Fig. 11 shows $(1/2\pi R_E^2)d(\cos\theta_v S)/d\theta_E$ where dS is a patch of surface area in the viewing range of ANITA at colatitude θ_E, as in Eq. (2).

The blue curve starts at $\theta_E = 0$, then increases as the annulus of area increases with θ_E, then decreases as $\cos\theta_v \to 0$ as the angle relative to the local $\hat{n}$ goes to 90°. The vertical blue dashed lines mark where $\beta_{\rm tr} = 40°$, 30°, 20°, and 10° are located in terms of θ_E. The red dotted line shows $\beta_{\rm tr} = 1°$. The interval $\beta_v = 30°$–40° contributes about 3% of the integral under the curve in Fig. 11. The interval $\beta_v = 0°$–10° makes up $\sim 64\%$ of the integral. This geometric effect cannot be overcome by modifications of sterile neutrino cross section and/or a large isotropic sterile neutrino flux.

A flaring point source of neutrinos could be responsible for the ANITA events as noted in, e.g. Refs. [38,41]. Other scenarios to produced anisotropies must overcome the geometric factor. For the angular range of the unusual events, given that $\beta_{\rm tr} \simeq \beta_v = 25°$–35° contributes $\sim 5\%$ to the geometric surface area, an anisotropy must have more

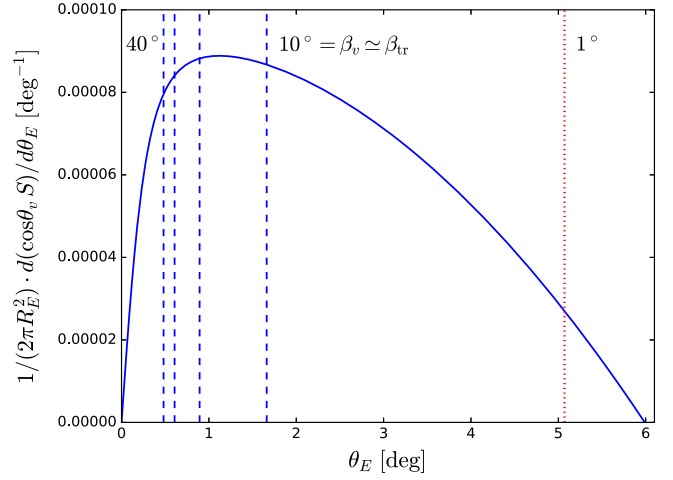FIG. 11. The differential effective area S as a function of the colatitude θ_E of a point on the surface in view, for $h = 35$ km. The blue vertical dashed lines, from left to right, show the corresponding β_v for $\beta_v = 40°, 30°, 20°$, and $10°$. The red dashed line corresponds to $\beta_v = 1°$.

than a factor of 20 in the angular range of the ANITA unusual events compared to skimming angles with $\beta_{\rm tr} \simeq \beta_v < 10°$.

III. DISCUSSION

Are there circumstances where tau decays in the atmosphere can produce more upward air shower events at ANITA for $\beta_{\rm tr} \simeq 30°$ than for $\beta_{\rm tr} \simeq 5°$? Figures 9 and 10 give a hint of the potential for relatively low energy $\sim 10^8$ GeV sterile neutrinos or other nonstandard model neutral particles to produce large $\beta_{\rm tr}$ signals compared to small $\beta_{\rm tr}$.

A key feature is that near the energy threshold of $\sim 10^8$ GeV for ANITA, large elevation angles are favored for detection. For diffuse neutrino fluxes that peak near ANITA's air shower threshold energy, the angular effect can be enhanced.

The Heaviside step function for the detection probability $P_{\rm det}$ in Eq. (6) requires

$$r_0 = v - s < 74 \text{ km} \frac{E_{\rm shr}}{10^8 \text{ GeV}}$$

$$v - 74 \text{ km} \frac{E_{\rm shr}}{10^8 \text{ GeV}} < s. \qquad (9)$$

The detection probability also requires that the altitude of the decay a satisfies

$$a < 6 \text{ km}. \qquad (10)$$

Figure 12 shows the distances v, s, and $s(a = 6 \text{ km})$ in Eqs. (9) and (10). The solid blue line shows the path length v between the tau exit point and ANITA as a function of tau
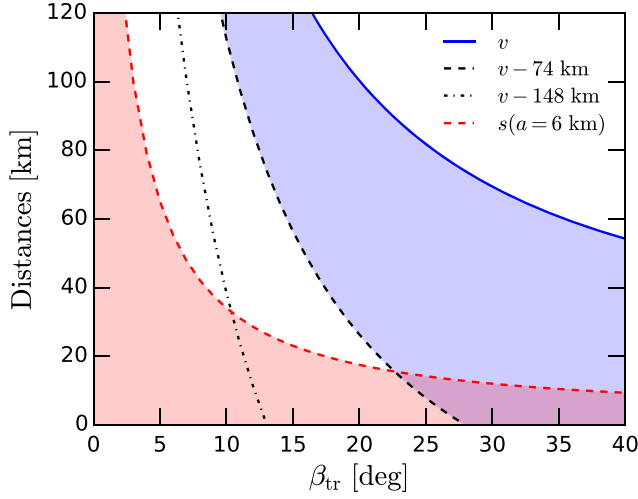
FIG. 12. The path length v of a trajectory with angle $\beta_{tr} \simeq \beta_v$ with respect to the horizon, to an altitude of $a = 35$ km.

elevation angle at the exit point. Since $E_{shr} = 0.98E_\tau$ in the approximate aperture evaluation, we equate the shower energy and tau energy in the discussion here. For $E_\tau = 10^8$ GeV, the difference between v and the distance s from the tau exit point to the decay must satisfy $v - s < 74$ km to be detectable. The blue dashed line in Fig. 12 shows $s = v - 74$ km as a function of β_{tr}. For a shower energy of 10^8 GeV to be detected, $s > v - 74$ km. The shaded blue region in the figure shows the allowed region for s given $E_\tau = 10^8$ GeV. For $\beta_{tr} = 1°$, $v = 567$ km, so a shower from a decay with $E_\tau = 10^8$ GeV ($\gamma c\tau \simeq 5$ km) will be very rarely detected. On the other hand, when $\beta_{tr} = 35°$, $v = 60.7$ km. All decay distances $s < v$ will satisfy the requirement in Eq. (9).

Our approximate effective aperture evaluation also requires the decay to occur below an altitude of $a = 6$ km. The path length s at an altitude of 6 km as a function of β_{tr} is represented by the red dashed line in Fig. 12. The shaded red region represents the allowed region of s that satisfies the altitude requirement. With this model of the effective aperture, only values of s in the overlapped red and blue shaded regions will be detected. For $E_\tau \simeq E_{shr} = 10^8$ GeV, Fig. 12 shows that the taus can only be detected at angles $\beta_{tr} \gtrsim 22°$. This is the effect that is seen in the behavior of the differential aperture for $E_\nu = 10^{8.25}$ GeV in Figs. 9 and 10.

As the shower energy increases, the allowed region for s also increases. The dot-dashed line in Fig. 12 shows the limit for $E_\tau = 2 \times 10^8$ GeV. The overlap of the region above the dot-dashed curve and below the red dashed curve is detectable. For this energy, $\beta_{tr} \gtrsim 10°$. Another factor of 2 increase in energy moves the minimum β_{tr} to $\sim 5°$.

The low energy $E_\tau \sim 10^8$ GeV air showers could, in principle, account for the large angle unusual ANITA events, but the effective aperture is small for both standard

model tau neutrinos and for sterile neutrinos. We illustrate the effect by evaluating ANITA's sensitivity to standard model tau neutrinos and sterile neutrinos. We use the effective aperture for $E_\nu = 10^{8.25}$ GeV $= 1.78 \times 10^8$ GeV which shows an enhanced event rate for large elevation angles of the tau.

We begin with standard model tau neutrinos. For this energy, $\langle A\Omega \rangle \simeq 3.6 \times 10^{-6}$ km^2 sr for the standard model. ANITA's sensitivity to a tau neutrino energy squared scaled flux with standard model interactions, based on an exclusion at the 90% unified confidence level in a decade of energy centered at $E_\nu = 10^{8.25}$ GeV for 115 days of ANITA I-IV flights, is

$$\text{Sensitivity} = \frac{2.44}{\ln(10)} \frac{1.78 \times 10^8 \text{ GeV}}{\langle A\Omega \rangle \times 9.9 \times 10^6 \text{ s}}$$

$$\simeq 5.3 \times 10^{-4} \frac{\text{GeV}}{\text{cm}^2 \text{ s sr}}. \qquad (11)$$

Standard model tau neutrino fluxes cannot be responsible for the ANITA unusual events as diffuse tau neutrino fluxes at this level are already excluded by IceCube [3] and Auger [10], as has already been emphasized recently by Romero-Wolf et al. in Ref. [26]. IceCube and Auger set upper bounds on the diffuse tau neutrino differential flux (assuming equal fluxes neutrino flavors) in the range of $E_\nu^2 \Phi(E_\nu) \sim 10^{-8} - 10^{-7}$ GeV/cm^2 ssr for $E_\nu = 10^8 - 10^{10}$ GeV.

The standard model tau neutrino effective aperture for ANITA rises quickly with energy, but as we have shown, this is accompanied by a larger predicted number of events for small β_{tr} compared to the large elevation angles of the ANITA events. For $E_\nu = 10^9$ GeV, $\langle A\Omega \rangle = 1.4 \times 10^{-2}$ km^2 sr. Putting aside the question of angular dependence, ANITA's sensitivity to tau neutrinos is of order $\sim 8 \times 10^{-7}$ GeV/cm^2 ssr for the decay of energy centered at $E_\nu = 10^9$ GeV, still more than an order of magnitude higher than current limit from Auger of $\sim 2 \times 10^{-8}$ GeV/cm^2 s sr [10].

For sterile neutrinos, the larger effective apertures lead to better sensitivities for ANITA. With $\epsilon_\nu = 0.1(0.01)$, $\langle A\Omega(10^{8.25} \text{ GeV}) \rangle \simeq 5.7 \times 10^{-5}(1.1 \times 10^{-5})$ km^2 sr. For a sensitivity as defined in Eq. (11), ANITA's sensitivity to sterile neutrinos with $\epsilon_\nu = 0.1(0.01)$ at $E_{\nu_s} = 10^{8.25}$ GeV is $3.3 \times 10^{-5}(1.7 \times 10^{-4})$ GeV/cm^2 s sr. For sterile neutrinos that oscillate with standard model neutrinos, the astrophysical tau flux is related to the sterile neutrino flux, so it is difficult to explain the unusual ANITA events with sterile neutrinos without over-predicting tau neutrino events in other detectors. In this paper, we are using the designation of sterile neutrino to denote a neutral particle with a cross section with nucleons to produce a tau that is smaller than the neutrino-nucleon cross section, so in principle, the flux of these particles does not have to be related to the diffuse cosmic neutrino flux.

One application of threshold energy enhancement of large angle events at ANITA is for monoenergetic sources. One example replaces the sterile neutrinos with χ's, discussed in a recent paper by Hooper *et al.* [39]. They propose that the unusual events at ANITA are Askaryan events from ultrahigh energy χ interactions, where supermassive dark matter $X_d \rightarrow \chi\chi$ decays in the galactic halo provide these monoenergetic, feebly interacting particles that have a cross section with nucleons that scales with the neutrino cross section $\sigma_{\chi N} = \epsilon_\chi \sigma_{\nu N}$. Using a Navarro-Frenk-White density profile of dark matter and a local density normalization of 0.4 GeV/cm^3, they find an integrated flux, averaged over 4π steradians, of [39]

$$F_\chi \simeq \frac{52}{\text{km}^2 \text{ yr sr}} \times \left(\frac{2 \times 10^{26} \text{ s}}{\tau_{X_d}}\right) \times \left(\frac{10^{11} \text{ GeV}}{m_{X_d}}\right), \quad (12)$$

in terms of the supermassive dark matter mass and lifetime. They constrain m_{X_d} and τ_{X_d} based on an observing time of 115 days of flight of ANITA I-IV, assuming no unusual events are found with ANITA IV. Hooper *et al.* found that the superheavy dark matter mass must be $m_{X_d} \gtrsim 1$–2×10^{10} GeV for small ϵ_χ [39] if the unusual events are Askaryan events. Our effective aperture can be carried over by substituting $E_\nu \rightarrow E_\chi$ and $\epsilon_\nu \rightarrow \epsilon_\chi$. If we set $\epsilon_\chi = 0.1(0.01)$ and $E_\chi = 10^{10}$ GeV, two Askaryan events for ANITA in 115 days correspond to $\sim 0.01(0.02)$ shower events in the same time period.

If the two unusual ANITA events are not Askaryan events but instead from upward air showers from χ interactions with nucleons to produce τ's, ANITA is sensitive to a different region of (m_{X_d}, τ_{X_d}) parameter space. For $E_\chi = 10^{8.25}$ GeV from the two body decay of X_d, $m_{X_d} = 3.56 \times 10^8$. For two events, the integrated flux is determined to be $F_\chi \simeq 1.1 \times 10^5/\text{km}^2$ yr sr for $\epsilon_\chi = 0.1$ and $F_\chi \simeq 5.8 \times 10^5/\text{km}^2$ yr sr for $\epsilon_\chi = 0.01$. For smaller fractions ϵ_χ, attenuation in the Earth does not play a role for χ propagation, so for $E_\chi = 10^{8.25}$ GeV,

$$F_\chi = \frac{5.8 \times 10^5}{\text{km}^2 \text{ yr sr}} \frac{0.01}{\epsilon_\chi} \quad (13)$$

to account for two ANITA events in 115 days.

Events from χ induced showers in the ice with $E_\chi = 10^{8.25}$ GeV are below ANITA's Askaryan energy threshold, so they would not be seen in Askaryan events. However, IceCube should see these high energy events. The number of downward IceCube events from χ interactions with $\epsilon_\chi = 0.1$ is estimated to be [39]

$$N \simeq 31/\text{yr} \quad \text{for } \epsilon_\chi = 0.1, \quad (14)$$

for these input parameters, using $V\Delta\Omega = 1$ km$^3 \times 2\pi$ sr. For smaller ϵ_χ,

$$N \simeq 16/\text{yr} \quad \text{for } \epsilon_\chi < 0.01. \quad (15)$$

The number of events does not depend on ϵ_χ for small values because F_χ scales as ϵ_χ^{-1} and the χN cross section scales with ϵ_χ. When attenuation in the Earth is negligible for χ transmission, the upward event rate should be independent of ϵ_χ.

The $\chi \rightarrow \tau$ events in IceCube would look like ν_τ production of τ's in the detector: there will be a hadronic shower with an associated tau. For $E_\chi = 10^{8.25}$ GeV, the average hadronic shower energy is ~ 36 PeV, and the average tau energy $\sim 1.4 \times 10^8$ GeV. Since $\gamma c \tau > 5$ km for the tau at this energy, the tau will look like a muon with energy loss that is a factor of $\sim m_\mu/m_\tau \sim 0.05$ relative to a muon. Thus, the taus associated with the ~ 36 PeV showers would appear to be ~ 8 PeV "muons." Muonlike tracks in the PeV energy range associated with cascades in the tens of PeV energy range, at a level of 16–31 events per year, are not observed, so this mass is excluded for X_d particles. Larger masses do not favor large elevation angles, and smaller masses put E_χ below detection thresholds.

IV. CONCLUSIONS

We have made an evaluation of the effective aperture for ANITA using a simplified model of the detection probability that is in reasonably good agreement with other results [26] for standard model tau neutrinos with perturbative neutrino-nucleon cross sections. A modified neutrino cross section, with high energy saturation effects modeled by color glass condensate suppression, does not have a large impact on the effective aperture. With a focus on the angular distribution of the effective sensitivity, we conclude that an isotropic flux of tau neutrinos cannot account for the large elevation angle ANITA event in the absence of skimming events. We concur with the authors of Ref. [26].

Our quantitative evaluation is extended to particles with cross sections suppressed by a factor of ϵ_ν relative to the standard model. We presented results for $\epsilon_\nu = 0.1$ and 0.01. The Monte Carlo simulation results for $\epsilon_\nu = 0.01$ can be simply rescaled by a factor of $\epsilon_\nu/0.01$ for $\epsilon_\nu < 0.01$, since we have demonstrated that the main angular effect is geometric, not related to attenuation in the Earth or detection if the energy is above $\sim 10^9$ GeV and $\beta_{\text{tr}} \gtrsim 5°$. Our results are more generally applicable to neutral particles incident on the Earth with feeble interactions that produce taus, as we showed with the supermassive dark matter model of Ref. [39].

We showed that near threshold for ANITA, the geometric effects of the detection condition favor large elevation angles for the tau, but the effective aperture is small. At higher energies, the small angles are more important to the overall aperture. For taus produced in the Earth by charged

currentlike interactions, our conclusion is that even with suppressed cross sections (e.g., for sterile neutrinos and other feebly interacting particles), tau decay air showers cannot account for the ANITA events and be reconciled with IceCube and/or Auger limits. Anisotropic sources that enhance event rates in the $\beta_{\rm tr} \simeq 25°–35°$ degree range must account for a factor of ~ 20 compared to the $0°–10°$ degree range based on geometric effects alone.

[1] K. Kotera and A. V. Olinto, The astrophysics of ultrahigh energy cosmic rays, Annu. Rev. Astron. Astrophys. **49**, 119 (2011).

[2] L. A. Anchordoqui, Ultra-high-energy cosmic rays, Phys. Rep. **801**, 1 (2019).

[3] M. G. Aartsen et al. (IceCube Collaboration), Differential limit on the extremely-high-energy cosmic neutrino flux in the presence of astrophysical background from nine years of IceCube data, Phys. Rev. D **98**, 062003 (2018).

[4] A. Albert et al. (ANTARES Collaboration), All-flavor search for a diffuse flux of cosmic neutrinos with nine years of ANTARES data, Astrophys. J. **853**, L7 (2018).

[5] M. Sanguineti (ANTARES and KM3NeT Collaborations), ANTARES and KM3NeT: The latest results of the neutrino telescopes in the mediterranean, Universe **5**, 65 (2019).

[6] P. Allison et al. (ARA Collaboration), Performance of two Askaryan Radio Array stations and first results in the search for ultrahigh energy neutrinos, Phys. Rev. D **93**, 082003 (2016).

[7] A. Anker et al. (ARIANNA Collaboration), Targeting ultra-high energy neutrinos with the ARIANNA experiment, Adv. Space Res., https://dx.doi.org/10.1016/j.asr.2019.06.016.

[8] A. Aab et al. (Pierre Auger Collaboration), Improved limit to the diffuse flux of ultrahigh energy neutrinos from the Pierre Auger observatory, Phys. Rev. D **91**, 092008 (2015).

[9] A. Aab et al. (Pierre Auger Collaboration), Multi-messenger physics with the Pierre Auger observatory, Front. Astron. Space Sci. **6**, 24 (2019).

[10] E. Zas (Pierre Auger Collaboration), Searches for neutrino fluxes in the EeV regime with the Pierre Auger observatory, Proc. Sci. ICRC2017 (**2018**) 972.

[11] R. U. Abbasi et al. (Telescope Array Collaboration), Search for ultra-high-energy neutrinos with the telescope array surface detector, arXiv:1905.03738.

[12] J. Alvarez-Muñiz et al. (GRAND Collaboration), The giant radio array for neutrino detection (GRAND): Science and design, Sci. China-Phys. Mech. Astron. **63**, 219501 (2020).

[13] A. N. Otte, Studies of an air-shower imaging system for the detection of ultrahigh-energy neutrinos, Phys. Rev. D **99**, 083012 (2019).

[14] A. Neronov, D. V. Semikoz, L. A. Anchordoqui, J. Adams, and A. V. Olinto, Sensitivity of a proposed space-based Cherenkov astrophysical-neutrino telescope, Phys. Rev. D **95**, 023004 (2017).

[15] A. V. Olinto et al., POEMMA: Probe of extreme multi-messenger astrophysics, Proc. Sci. ICRC2017 (**2018**) 542.

[16] P. W. Gorham et al. (ANITA Collaboration), Constraints on the diffuse high-energy neutrino flux from the third flight of ANITA, Phys. Rev. D **98**, 022001 (2018).

[17] P. W. Gorham et al. (ANITA Collaboration), Constraints on the ultra-high energy cosmic neutrino flux from the fourth flight of ANITA, Phys. Rev. D **99**, 122001 (2019).

[18] P. W. Gorham et al. (ANITA Collaboration), Characteristics of Four Upward-pointing Cosmic-ray-like Events Observed with ANITA, Phys. Rev. Lett. **117**, 071101 (2016).

[19] P. W. Gorham et al., Observation of an Unusual Upward-going Cosmic-ray-like Event in the Third Flight of ANITA, Phys. Rev. Lett. **121**, 161102 (2018).

[20] J. G. Learned and S. Pakvasa, Detecting tau-neutrino oscillations at PeV energies, Astropart. Phys. **3**, 267 (1995).

[21] R. Gandhi, C. Quigg, M. H. Reno, and I. Sarcevic, Ultra-high-energy neutrino interactions, Astropart. Phys. **5**, 81 (1996).

[22] R. Gandhi, C. Quigg, M. H. Reno, and I. Sarcevic, Neutrino interactions at ultrahigh-energies, Phys. Rev. D **58**, 093009 (1998).

[23] Y. S. Jeong and M. H. Reno, Quark mass effects in high energy neutrino nucleon scattering, Phys. Rev. D **81**, 114012 (2010).

[24] A. Connolly, R. S. Thorne, and D. Waters, Calculation of high energy neutrino-nucleon cross sections and uncertainties using the MSTW parton distribution functions and implications for future experiments, Phys. Rev. D **83**, 113009 (2011).

[25] A. Cooper-Sarkar, P. Mertsch, and S. Sarkar, The high energy neutrino cross-section in the Standard Model and its uncertainty, J. High Energy Phys. 08 (2011) 042.

[26] A. Romero-Wolf et al., Comprehensive analysis of anomalous ANITA events disfavors a diffuse tau-neutrino flux origin, Phys. Rev. D **99**, 063011 (2019).

[27] D. B. Fox, S. Sigurdsson, S. Shandera, P. Mészáros, K. Murase, M. Mostafá, and S. Coutu, The ANITA anomalous events as signatures of a beyond Standard Model particle, and supporting observations from IceCube, arXiv:1809.09615.

[28] L. Heurtier, Y. Mambrini, and M. Pierre, Dark matter interpretation of the ANITA anomalous events, Phys. Rev. D **99**, 095014 (2019).

[29] K. D. de Vries and S. Prohira, Coherent Transition Radiation from the Geomagnetically-Induced Current in Cosmic-Ray Air Showers: Implications for the Anomalous Events Observed by ANITA, Phys. Rev. Lett. **123**, 091102 (2019).

[30] I. M. Shoemaker, A. Kusenko, P. K. Munneke, A. Romero-Wolf, D. M. Schroeder, and M. J. Siegert, Reflections on the anomalous ANITA events: The antarctic subsurface as a possible explanation, arXiv:1905.02846.

[31] I. Esteban, J. Lopez-Pavon, I. Martinez-Soler, and J. Salvado, Looking at the axionic dark sector with ANITA, arXiv:1905.10372.

[32] A. Connolly, P. Allison, and O. Banerjee, On ANITA's sensitivity to long-lived, charged massive particles, arXiv:1807.08892.

[33] J. H. Collins, P. S. Bhupal Dev, and Y. Sui, R-parity violating supersymmetric explanation of the anomalous events at ANITA, Phys. Rev. D **99**, 043009 (2019).

[34] B. Chauhan and S. Mohanty, Leptoquark solution for both the flavor and ANITA anomalies, Phys. Rev. D **99**, 095018 (2019).

[35] L. A. Anchordoqui and I. Antoniadis, Supersymmetric sphaleron configurations as the origin of the perplexing ANITA events, Phys. Lett. B **790**, 578 (2019).

[36] L. A. Anchordoqui, V. Barger, J. G. Learned, D. Marfatia, and T. J. Weiler, Upgoing ANITA events as evidence of the *CPT* symmetric universe, Lett. High Energy Phys. **1**, 13 (2018).

[37] L. Heurtier, D. Kim, J.-C. Park, and S. Shin, Explaining the ANITA anomaly with inelastic boosted dark matter, Phys. Rev. D **100**, 055004 (2019).

[38] J. M. Cline, C. Gross, and W. Xue, Can the ANITA anomalous events be due to new physics, Phys. Rev. D **100**, 015031 (2019).

[39] D. Hooper, S. Wegsman, C. Deaconu, and A. Vieregg, Superheavy dark matter and ANITA's anomalous events, Phys. Rev. D **100**, 043019 (2019).

[40] G.-Y. Huang, Sterile neutrinos as a possible explanation for the upward air shower events at ANITA, Phys. Rev. D **98**, 043019 (2018).

[41] J. F. Cherry and I. M. Shoemaker, Sterile neutrino origin for the upward directed cosmic ray showers detected by ANITA, Phys. Rev. D **99**, 063016 (2019).

[42] M. H. Reno, J. F. Krizmanic, and T. M. Venters, Cosmic tau neutrino detection via Cherenkov signals from air showers from Earth-emerging taus, arXiv:1902.11287 [Phys. Rev. D (to be published)].

[43] L. D. McLerran and R. Venugopalan, Computing quark and gluon distribution functions for very large nuclei, Phys. Rev. D **49**, 2233 (1994).

[44] J. Jalilian-Marian, A. Kovner, L. D. McLerran, and H. Weigert, The Intrinsic glue distribution at very small x, Phys. Rev. D **55**, 5414 (1997).

[45] L. D. McLerran and R. Venugopalan, Fock space distributions, structure functions, higher twists and small x, Phys. Rev. D **59**, 094002 (1999).

[46] Y. V. Kovchegov, NonAbelian Weizsacker-Williams field and a two-dimensional effective color charge density for a very large nucleus, Phys. Rev. D **54**, 5463 (1996).

[47] Y. V. Kovchegov, Quantum structure of the nonAbelian Weizsacker-Williams field for a very large nucleus, Phys. Rev. D **55**, 5445 (1997).

[48] E. M. Henley and J. Jalilian-Marian, Ultra-high energy neutrino-nucleon scattering and parton distributions at small x, Phys. Rev. D **73**, 094004 (2006).

[49] P. Motloch, N. Hollon, and P. Privitera, On the prospects of ultra-high energy cosmic rays detection by high altitude antennas, Astropart. Phys. **54**, 40 (2014).

[50] A. Romero-Wolf *et al.* (ANITA Collaboration), Upward-pointing cosmic-ray-like events observed with ANITA, Proc. Sci., ICRC2017 (**2018**) 935.

[51] S. Dulat, T.-J. Hou, J. Gao, M. Guzzi, J. Huston, P. Nadolsky, J. Pumplin, C. Schmidt, D. Stump, and C. P. Yuan, New parton distribution functions from a global analysis of quantum chromodynamics, Phys. Rev. D **93**, 033006 (2016).

[52] S. I. Dutta, M. Reno, I. Sarcevic, and D. Seckel, Propagation of muons and taus at high-energies, Phys. Rev. D **63**, 094020 (2001).

[53] H. Abramowicz, E. M. Levin, A. Levy, and U. Maor, A Parametrization of $\sigma_T(\gamma^* p)$ above the resonance region $Q^2 \geq 0$, Phys. Lett. B **269**, 465 (1991).

[54] H. Abramowicz and A. Levy, The ALLM parameterization of $\sigma(tot)(\gamma^* p)$: An update, arXiv:hep-ph/9712415.

[55] F. Halzen and D. Saltzberg, Tau-Neutrino Appearance with a 1000 Megaparsec Baseline, Phys. Rev. Lett. **81**, 4305 (1998).

[56] S. Iyer, M. H. Reno, and I. Sarcevic, Searching for muon-neutrino → tau-neutrino oscillations with extragalactic neutrinos, Phys. Rev. D **61**, 053003 (2000).

[57] S. I. Dutta, M. H. Reno, and I. Sarcevic, Tau neutrinos underground: Signals of muon-neutrino → tau neutrino oscillations with extragalactic neutrinos, Phys. Rev. D **62**, 123001 (2000).

[58] F. Becattini and S. Bottai, Extreme energy neutrino(tau) propagation through the Earth, Astropart. Phys. **15**, 323 (2001).

[59] J. F. Beacom, P. Crotty, and E. W. Kolb, Enhanced signal of astrophysical tau neutrinos propagating through earth, Phys. Rev. D **66**, 021302 (2002).

[60] J. Alvarez-Muñiz, W. R. Carvalho, A. L. Cummings, K. Payet, A. Romero-Wolf, H. Schoorlemmer, and E. Zas, Comprehensive approach to tau-lepton production by high-energy tau neutrinos propagating through the Earth, Phys. Rev. D **97**, 023021 (2018); Erratum, Phys. Rev. D **99**, 069902(E) (2019).

[61] G. Domokos and S. Kovesi-Domokos, Observation of UHE interactions neutrinos from outer space, AIP Conf. Proc. **433**, 390 (1998).

[62] G. Domokos and S. Kovesi-Domokos, Observation of ultrahigh energy neutrino interactions by orbiting detectors, arXiv:hep-ph/9805221.

[63] D. Fargion, Discovering ultra high energy neutrinos by horizontal and upward tau air-showers: Evidences in terrestrial gamma flashes, Astrophys. J. **570**, 909 (2002).

[64] D. Fargion, P. De Sanctis Lucentini, and M. De Santis, Tau air showers from earth, Astrophys. J. **613**, 1285 (2004).

[65] D. Fargion, Tau neutrino astronomy, in *Beyond the Desert, Proceedings of the 4th International Conference, Particle*

Physics Beyond the Standard Model, BEYOND 2003, Castle Ringberg, Tegernsee, Germany, 2003, edited by H.-V. Klapdor-Kleingrothaus (Springer, Berlin, 2004), pp. 831–856.

[66] X. Bertou, P. Billoir, O. Deligny, C. Lachaud, and A. Letessier-Selvon, Tau neutrinos in the Auger observatory: A new window to UHECR sources, Astropart. Phys. **17,** 183 (2002).

[67] J. L. Feng, P. Fisher, F. Wilczek, and T. M. Yu, Observability of Earth Skimming Ultrahigh-Energy Neutrinos, Phys. Rev. Lett. **88,** 161102 (2002).

[68] C. Lachaud, X. Bertou, P. Billoir, O. Deligny, and A. Letessier-Selvon, Probing the GZK barrier with UHE tau neutrinos, Nucl. Phys. B, Proc. Suppl. **110,** 525 (2002).

[69] S. Bottai and S. Giurgola, UHE and EHE neutrino induced taus inside the Earth, Astropart. Phys. **18,** 539 (2003).

[70] G. W. Hou and M. Huang, Expected performance of a neutrino telescope for seeing AGN/GC behind a mountain, https://dx.doi.org/10.1142/97898127768600006.

[71] J.-J. Tseng, T.-W. Yeh, H. Athar, M. A. Huang, F.-F. Lee, and G.-L. Lin, The energy spectrum of tau leptons induced by the high energy Earth-skimming neutrinos, Phys. Rev. D **68,** 063003 (2003).

[72] C. Aramo, A. Insolia, A. Leonardi, G. Miele, L. Perrone, O. Pisanti, and D. V. Semikoz, Earth-skimming UHE Tau neutrinos at the fluorescence detector of Pierre Auger observatory, Astropart. Phys. **23,** 65 (2005).

[73] S. I. Dutta, Y. Huang, and M. H. Reno, Tau neutrino propagation and tau energy loss, Phys. Rev. D **72,** 013005 (2005).

[74] Y. Asaoka and M. Sasaki, Cherenkov tau shower earth-skimming method for PeV-EeV tau neutrino observation with ashra, Astropart. Phys. **41,** 7 (2013).

[75] S. Palomares-Ruiz, A. Irimia, and T. J. Weiler, Acceptances for space-based and ground-based fluorescence detectors, and inference of the neutrino-nucleon cross-section above 10^{19}-ev, Phys. Rev. D **73,** 083003 (2006).